$\mathcal{PT}$-symmetric magnon laser in cavity optomagnonics

Bao Wang,[1,*] Xiao Jia,[1] Xiao-Hu Lu,[1] and Hao Xiong[2,†]
[1]*School of Information Engineering, Nanyang Institute of Technology, Nanyang 473004, China*
[2]*School of Physics, Huazhong University of Science and Technology, Wuhan 430074, China*

(Received 10 January 2022; revised 23 March 2022; accepted 25 April 2022; published 5 May 2022)

Nonlinear magnonics based on the coupling of magnons and optical photons has become a crucial topic in the quantum magnonic field. Here, we demonstrate the magnon laser, the analog of the optical laser in magnonics, in a parity-time ($\mathcal{PT}$) symmetric cavity optomagnonical system involving active and passive optical whispering gallery modes and the magnon mode. We show that the stimulated emitted magnon number can be coherently amplified above a threshold driving power in the $\mathcal{PT}$-symmetric regime where the splitting of optical supermodes is resonant with the magnon frequency, indicating the occurrence of the magnon laser. And this magnon laser action can work with low threshold when the system approaches the optical gain-loss balance and when increasing the optomagnonic coupling. Furthermore, the frequency of the magnon laser can be continuously tuned by adjusting the applied magnetic field strength, which is a distinct feature compared to the photon or phonon amplification by stimulated emission. The study of the $\mathcal{PT}$-symmetric magnon laser may promote the intersection and merging of various disciplines like non-Hermitian physics and quantum magnonics, and provide the theoretical basis and reference for the research and development of new frequency-tunable laser devices.

DOI: 10.1103/PhysRevA.105.053705

I. INTRODUCTION

A spin wave refers to collective excitation of magnetization in ordered magnets, and its propagation does not require the directional motion of electrons, making it a crucial information carrier in modern information technology [1]. A magnon is the spin wave quantum and possesses excellent nonlinearity and quantum properties [2–8]. Recent experiments have shown that a yttrium iron garnet (YIG) sphere holds extremely high spin density $\rho \sim 4.22 \times 10^{27}$ m^{-3}, which results in strong and even ultrastrong coupling between microwave photons and magnons based on magnetic dipole interaction due to the mode anticrossing effect and the emergence of magnon polaritons in the cavity magnonics [6,7]. The YIG crystal has a high Curie temperature that is up to 559 K and can preserve ferromagnetic peculiarity at room temperature; in addition, its operational dissipation is very low, achieving a long quantum coherence time [1,5]. These merits and powerful compatibility promote the emergence of new hybrid quantum system for quantum information processing based on magnons, including the coupling between magnons and magnons [9], microwave photons [3,10], phonons [11–14], and a superconducting qubit [15–17].

Currently, cavity optomagnonics [18–21], which describes the magneto-optical coupling between optical whispering gallery modes (WGMs) and magnon modes in the ferrimagnet YIG sphere, has attracted extensive attention in the quantum information field and has achieved many exciting advances, for instance, coherent optical-to-microwave conversion [22,23], Brillouin light scattering [20,21,24], magnon entanglement [25], magnon induced transparency [26,27], magnon induced photonic frequency combs [28], and chaos [29,30]. On the other hand, non-Hermitian cavity magnonics—including the concept of $\mathcal{PT}$ symmetry, that makes a non-Hermitian physical system a real eigenvalue spectrum, and the exceptional point (EP, $\mathcal{PT}$-symmetry phase transition point) [31–33]—has aroused considerable interest and emerges as a new frontier in the magnonic field. Many interesting and useful phenomena—such as observing the EPs in non-Hermitian systems [34,35], controllable EPs and bound states in the continuum (BICs) in anti-$\mathcal{PT}$-symmetric cavity magnonic systems [36], and highly sensitive magnetometers with sensitivity approaching about 10^{-15} T/$\sqrt{\text{Hz}}$ in $\mathcal{PT}$-symmetric cavity magnonic systems—have been reported [37]. As a significant nonlinear magnonic phenomenon, the magnon laser, performing coherent amplification of stimulated emission of magnons, has been discussed based on Brillouin light scattering [38,39]. Achieving frequency tuning functionality is of practical significance for laser devices. Many experimental proposals have been presented to affect the frequency of light, for instance changing the refractive index when light is inside the cavity [40] and employing superconducting microwave resonators to realize frequency tuning [41]. More importantly, the magnetization of a YIG sphere is greatly tunable by external magnetic field, with magnon frequency ranging from gigahertz (GHz) to terahertz (THz) [42]. This merit, combined with $\mathcal{PT}$-symmetric cavity optomagnonics, makes the magnon laser with adjustable frequency possible.

Optical lasers, performing at the same frequency and phase, namely, coherent photons in quantum mechanical language, have extremely wide applications in modern science.

*baowang@hust.edu.cn
†haoxiong@hust.edu.cn

Taking into consideration the analogy between magnon and photon, the analog of the optical laser in an optomagnonical system is an interesting and practical subject. In the present work, we investigate the steady-state dynamic properties of a $\mathcal{PT}$-symmetric cavity optomagnonical system excited by an input light field and obtain the analytical expression for the stimulated emission of magnon number based on the adiabatic elimination method that is proposed to handle the stimulated emission of phonons in optomechanics successfully [31,43]. The threshold power and frequency regulation of the $\mathcal{PT}$-symmetric magnon laser in different parameter configurations are discussed. We show that the stimulated emitted magnon number can be coherently amplified in a certain parameter condition within the $\mathcal{PT}$-symmetric regime, namely, $\mathcal{PT}$-symmetric magnon laser action occurs. And the magnon-laser threshold can be decreased by increasing the optical gain-loss ratio and the optomagnonic coupling strength. Moreover, the frequency of magnon laser can be continuously adjusted by regulating the applied magnetic field strength. The matching condition for $\mathcal{PT}$-symmetric magnon laser generation has been analyzed in detail. In addition, we theoretically explored the possibility of observing the $\mathcal{PT}$-symmetric magnon laser under the current experimental conditions. Our results provide a promising method for engineering a magnon-photon converter [22,23], manipulating a coherent magnon source [44], and developing flexible magnon laser devices.

This paper is organized suitably as follows. We give a detailed description of the $\mathcal{PT}$-symmetric cavity optomagnonical system in Sec. II, where the system Hamiltonian and a group of dynamics equations are given and simplified safely within the semiclassical approximation. We solve these nonlinear equations analytically by means of the adiabatic elimination method. In Sec. III, we discuss the features of a magnon laser in a $\mathcal{PT}$-symmetric cavity optomagnonical system in detail. Finally, the results we obtained and our conclusions are summarized in Sec. IV.

II. PHYSICAL SETUP AND DYNAMICAL EQUATION

As shown in Fig. 1(a), we consider a $\mathcal{PT}$-symmetric cavity optomagnonical system, consisting of an active WGM microcavity and a micrometer-scale ferrimagnet YIG sphere. In this physical model, the YIG sphere is uniformly magnetized by a static magnetic field $\mathbf{B}_z = B\mathbf{e}_z$ in the z direction and supports the passive optical WGMs and magnon modes such as the Kittel mode [20,23]. The total Hamiltonian reads

$$\begin{aligned}\hat{H} &= \hbar\omega_c(\hat{a}_1^\dagger\hat{a}_1 + \hat{a}_2^\dagger\hat{a}_2) + \hbar J(\hat{a}_1^\dagger\hat{a}_2 + \hat{a}_2^\dagger\hat{a}_1) \\ &\quad + i\hbar\sqrt{\kappa_1/2}\,\Omega_d(\hat{a}_1^\dagger e^{-i\omega_d t} - \hat{a}_1 e^{i\omega_d t}) + \hat{H}_{\rm spin}, \end{aligned} \tag{1}$$

where $\hat{a}_1$ ($\hat{a}_1^\dagger$) and $\hat{a}_2$ ($\hat{a}_2^\dagger$) are the annihilation (creation) operators of the active cavity mode and the passive cavity mode, respectively. The active WGM $\hat{a}_1$ couples to the passive mode $\hat{a}_2$ (with the same resonance frequency ω_c) with the coupling strength J via the optical tunneling effect and is driven with frequency ω_d (setting $\omega_d = \omega_c$) and amplitude $\Omega_d = \sqrt{P_{\rm in}/\hbar\omega_d}$ with $P_{\rm in}$ being the input power. The cavity $\hat{a}_1$ is fabricated from silica doped with Er^{3+} ions, and the optical gain can be acquired by optically pumping the Er^{3+} ions [45,46]. The magnon-photon coupling due to the

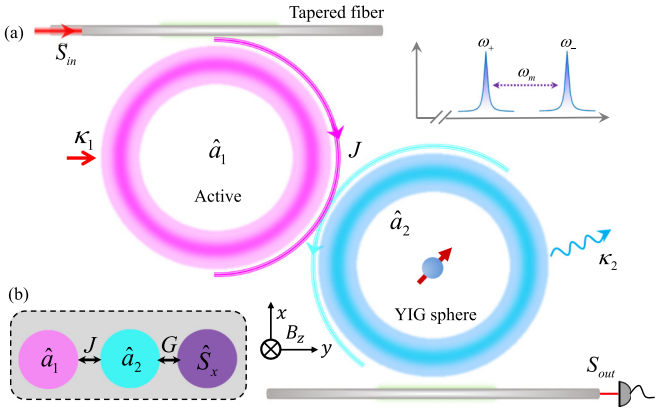

FIG. 1. (a) Schematic diagram of the $\mathcal{PT}$-symmetric cavity optomagnonical system. The ferrimagnet YIG sphere supports optical WGM $\hat{a}_2$ and magnon mode $\hat{S}_x$ and couples to an active optical WGM microcavity $\hat{a}_1$. The input light evanescently couples to the active optical WGM via a tapered fiber. The two optical supermodes ω_+ and ω_- caused by the coupled optical WGMs interact with the magnon mode with frequency ω_m, i.e., $\omega_+ \leftrightarrow \omega_- + \omega_m$. (b) The physical model of three-mode interaction.

Faraday effect is captured by the interaction of the circularly polarized optical WGM and the x component of the collective spin $\hat{\mathbf{S}} \equiv (\hat{S}_x, \hat{S}_y, \hat{S}_z)$ [20,42]. The Hamiltonian of the optomagnonic interaction can be well written as $\hat{H}_{\rm int} = \hbar G\hat{S}_x\hat{a}_2^\dagger\hat{a}_2$, where the coupling strength $G = \frac{1}{S}\frac{c\vartheta_F}{4\sqrt{\varepsilon}}$ [20], also known as parametric optomagnonic coupling, with the total spin number S of the YIG sphere, the vacuum speed of light c, the Faraday rotation ϑ_F per unit length, and the relative permittivity ε. The frequency of the magnon mode can be expressed by $\omega_m = \gamma H_0$, wherein $\gamma/2\pi = 28$ GHz/T is the gyromagnetic ratio and H_0 denotes the magnetic field strength [6]. The Hamiltonian of the spin mode can be described by $\hat{H}_m = -\hbar\omega_m\hat{S}_z$. Consequently, $\hat{H}_{\rm spin} = \hat{H}_m + \hat{H}_{\rm int} = -\hbar\omega_m\hat{S}_z + \hbar G\hat{S}_x\hat{a}_2^\dagger\hat{a}_2$. In a word, the cavity modes $\hat{a}_1$, $\hat{a}_2$ and spin mode $\hat{S}_x$ form a tripartite cascade model, as shown in Fig. 1(b). Based on the huge spin density, the expressions $\hat{S}_x = \sqrt{S/2}(\hat{m} + \hat{m}^\dagger)$ and $\hat{S}_z = S - \hat{m}^\dagger\hat{m}$ can be yielded by the Holstein-Primakoff transform [47], where $\hat{S}_x$ and $\hat{S}_z$ represent the x and z components of the spin operator, respectively. Then $\hat{H}_{\rm spin} = \hbar\omega_m\hat{m}^\dagger m + \hbar G\sqrt{S/2}\,\hat{a}_2^\dagger\hat{a}_2(\hat{m} + \hat{m}^\dagger)$, which is the starting point of our following discussion; that is, we can replace the spin $\hat{\mathbf{S}}$ with the magnon m.

Based on the above Hamiltonian, in a frame rotating with frequency ω_d, the system dynamics can be well described by the Heisenberg-Langevin equations ($\dot{\hat{A}} = \frac{i}{\hbar}[\hat{H}, \hat{A}]$) via the unitary transformation $\mathbb{U}(t) = \exp[-i\omega_d(\hat{a}_1^\dagger\hat{a}_1 + \hat{a}_2^\dagger\hat{a}_2)t]$:

$$\dot{a}_1 = \kappa_1/2a_1 - iJa_2 + \sqrt{\kappa_1/2}\Omega_d, \tag{2a}$$

$$\dot{a}_2 = -\kappa_2/2a_2 - iJa_1 - iG\sqrt{S/2}a_2(m^* + m), \tag{2b}$$

$$\dot{m} = -i\omega_m m - \gamma_m/2m - iG\sqrt{S/2}a_2^* a_2, \tag{2c}$$

where κ_1, κ_2, and γ_m are, respectively, the optical gain of the active cavity mode $\hat{a}_1$, the optical decay of the passive cavity mode $\hat{a}_2$, and the decay rate of the magnon mode. Within the semiclassical approximation, all operators are reduced to

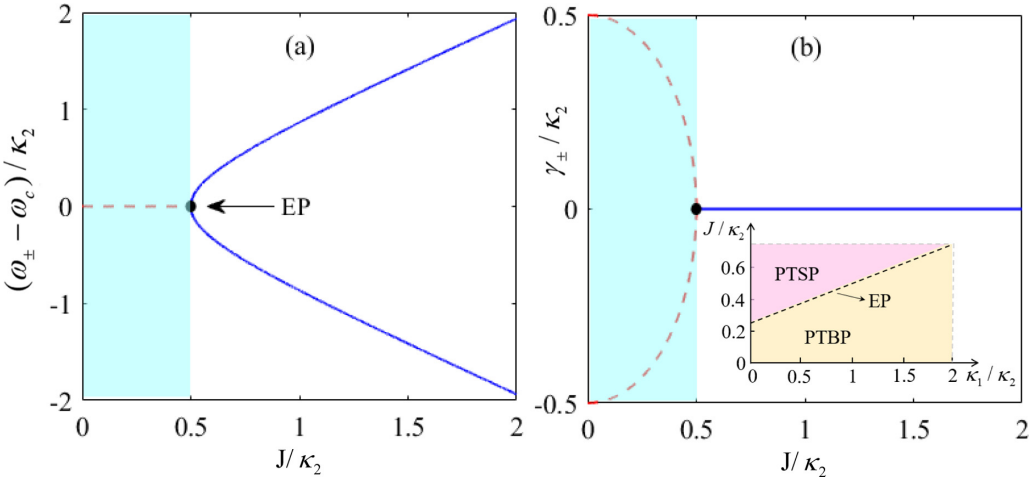

FIG. 2. (a) Mode splitting $(\omega_\pm - \omega_c)/\kappa_2$ and (b) linewidth $\gamma_\pm/\kappa_2$ of the eigenmodes vary with the optical tunneling rate J/κ_2 under the condition of $\kappa_1 = \kappa_2$. Inset map in (b): The phase diagram displays the EP, $\mathcal{PT}$-symmetry phase (PTSP), and $\mathcal{PT}$-symmetry-breaking phase (PTBP).

their expectation values in the case of considering the mean response of the system, viz., $a_{1(2)} = \langle \hat{a}_{1(2)} \rangle$, $m = \langle \hat{m} \rangle$, as well as $m^* = \langle \hat{m}^\dagger \rangle$, and the quantum correlations and noise terms can be safely dropped [48,49]. In addition, the mean-field approximation by factorizing averages, i.e., $\langle \hat{m}^\dagger \hat{m} \rangle = m^* m$, is used to deal with the nonlinear term $iG\sqrt{S/2}\, a_2^* a_2$. Accordingly, the steady-state solutions provided by the input light $P_{\rm in}$ are, respectively, $a_{1s} = -\sqrt{\kappa_1/2}\Omega_d/[\kappa_1/2 - J^2/(\kappa_2/2 + i\phi_0)]$, $a_{2s} = iJ\sqrt{\kappa_1/2}\,\Omega_d/(\kappa_1\kappa_2/4 - J^2 + i\kappa_1\phi_0/2)$, and $m_s = -iG\sqrt{S/2}\,|a_{2s}|^2/(i\omega_m + \gamma_m/2)$, where $\phi_0 = G\sqrt{S/2}(m_s^* + m_s)$.

Before proceeding further, let us illustrate the physical mechanism of the EP and $\mathcal{PT}$-symmetry phase transition. The non-Hermitian Hamiltonian $\hbar\omega_c(\hat{a}_1^\dagger \hat{a}_1 + i\kappa_1/2) + \hbar\omega_c(\hat{a}_2^\dagger \hat{a}_2 - i\kappa_2/2) + \hbar J(\hat{a}_1^\dagger \hat{a}_2 + \hat{a}_2^\dagger \hat{a}_1)$ can be straightforwardly diagonalized as $\hbar(\omega_+ + i\gamma_+)\hat{a}_+^\dagger \hat{a}_+ + \hbar(\omega_- + i\gamma_-)\hat{a}_-^\dagger \hat{a}_-$ via a Bogoliubov transformation [50], with $\omega_\pm = \omega_c \pm \sqrt{J^2 - (\kappa_1 + \kappa_2)^2/16}$ and $\gamma_\pm = (\kappa_1 - \kappa_2)/4$ being the eigenfrequencies and decay of the two eigenmodes $\hat{a}_\pm = (\hat{a}_1 \pm \hat{a}_2)/\sqrt{2}$, also called optical supermodes.

In Fig. 2, we plot the mode splitting and linewidth of the optical supermodes as a function of the optical tunneling rate J/κ_2. As can be seen from Figs. 2(a) and 2(b), for the case of $J > (\kappa_1 + \kappa_2)/4$, the two eigenvalues are real and nondegenerate, and simultaneously the corresponding dissipation rates $\gamma_\pm = (\kappa_1 - \kappa_2)/4$ are degenerate, indicating the system is in the $\mathcal{PT}$-symmetry phase. The splitting width $\Delta\omega$ of the two modes $\omega_\pm$ is $2\sqrt{J^2 - (\kappa_1 + \kappa_2)^2/16}$. When $J < (\kappa_1 + \kappa_2)/4$, the eigenvalues coalesce, i.e., $\omega_\pm = \omega_c$, and the corresponding dissipation rates are $\gamma_\pm = (\kappa_1 - \kappa_2)/4 \pm \sqrt{J^2 - (\kappa_1 + \kappa_2)^2/16}$, corresponding to the $\mathcal{PT}$-symmetry-breaking phase. The inset map in Fig. 2(b) presents the $\mathcal{PT}$-symmetry phase transition diagram in terms of J/κ_2 and κ_1/κ_2, where the black dashed line caused by $J = (\kappa_1 + \kappa_2)/4$ represents the EP. The above and following areas of EP indicate the $\mathcal{PT}$-symmetry phase and $\mathcal{PT}$-symmetry-breaking phase respectively. Subsequently, we can analyze the physical process in the eigenstate representation [31–33].

By applying the rotating-wave approximation, we can derive the Hamiltonian in the new representation, yielding

$$\hat{\mathcal{H}} = \hbar\omega_+ \hat{a}_+^\dagger \hat{a}_+ + \hbar\omega_- \hat{a}_-^\dagger \hat{a}_- + \hbar\omega_m \hat{m}^\dagger \hat{m} - \frac{\hbar G\sqrt{S/2}}{2}(\hat{a}_-^\dagger \hat{a}_+ \hat{m}^\dagger + \hat{a}_+^\dagger \hat{a}_- \hat{m}). \tag{3}$$

The detailed derivation is given in Eqs. (A1)–(A3) of the Appendix. Based on the above Hamiltonian, the system dynamics can be well described by the Heisenberg-Langevin equations ($\dot{\hat{A}} = \frac{i}{\hbar}[\hat{H}, \hat{A}]$)

$$\frac{d\psi}{dt} = \mathcal{M}\psi + \varrho, \tag{4}$$

where $\psi = (\hat{m}, \hat{\Phi})^T$, $\hat{\Phi} = \hat{a}_-^\dagger \hat{a}_+$ is the optical inversion operator with $\hat{a}_\pm = (\hat{a}_1 \pm \hat{a}_2)/\sqrt{2}$, the coefficient matrix

$$\mathcal{M} = \begin{pmatrix} -i\omega_m - \gamma_m/2 & iG\sqrt{S/2}/2 \\ -iG\sqrt{S/2}\Delta N/2 & -i\Delta\omega - \gamma'/2 \end{pmatrix},$$

$\Delta N = \hat{a}_+^\dagger \hat{a}_+ - \hat{a}_-^\dagger \hat{a}_-$, $\Delta\omega = 2\sqrt{J^2 - (\kappa_1 + \kappa_2)^2/16}$, $\gamma' = \kappa_1 - \kappa_2$, and $\varrho = (\hat{m}_{\rm in}, \hat{\Phi}_{\rm in})^T$ are the noise operators including quantum and thermal noise and their mean values are zero, i.e., $\langle \hat{m}_{\rm in}(t) \rangle = 0$ and $\langle \hat{\Phi}_{\rm in}(t) \rangle = 0$. The correlation functions of the noise term of the magnon mode are given by $\langle \hat{m}_{\rm in}(t)\hat{m}_{\rm in}^\dagger(t') \rangle = [m_{\rm th}(\omega_m) + 1]\delta(t - t')$ and $\langle \hat{m}_{\rm in}^\dagger(t)\hat{m}_{\rm in}(t') \rangle = m_{\rm th}(\omega_m)\delta(t - t')$ where the average numbers of the equilibrium thermal magnon $m_{\rm th}(\omega_m) = [\exp(\hbar\omega_m/k_B T) - 1]^{-1}$ with k_B being the Boltzmann constant and T being the environmental temperature [51]. Applying the semiclassical approximation, all operators are reduced to their expectation values, viz., $m = \langle \hat{m} \rangle$ and $\Phi = \langle \hat{\Phi} \rangle$, and the quantum noise terms can be safely dropped. Then the Heisenberg-Langevin equations (4) can be converted into the following forms by transferring the variables m and Φ to the rotating frame, i.e., $\tilde{m} = me^{i\omega_m t}$ and $\tilde{\Phi} = \Phi e^{i\Delta\omega t}$ [see

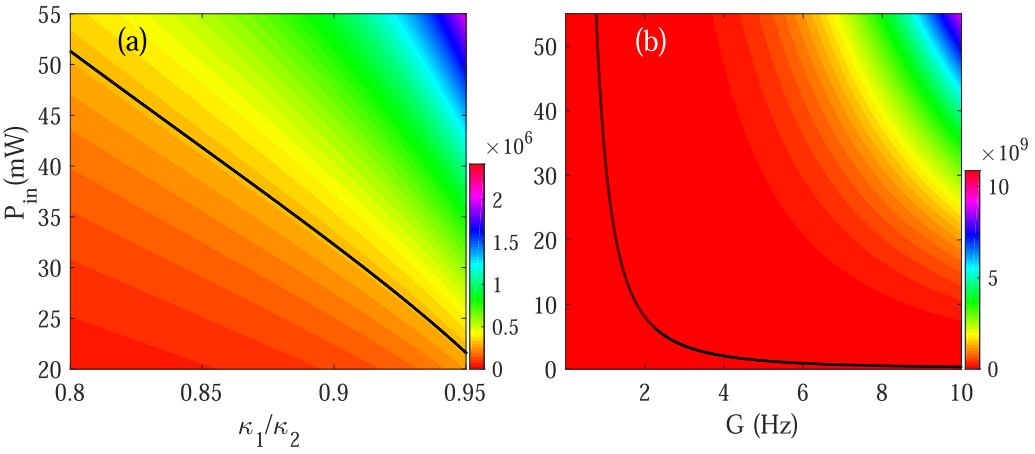

FIG. 3. The magnon gain $\mathcal{G}$ as a function of the incident power P_{in} and (a) optical gain-loss ratio κ_1/κ_2 and (b) the optomagnonic coupling strength G. The black solid lines represent the threshold power P_{th} evolved by (a) κ_1/κ_2 and (b) G subject to $\mathcal{G} = \gamma_m/2$. We use $G = 1$ Hz [53–55] in (a) and $\kappa_1/\kappa_2 = 0.9$ in (b), and the other system parameters are $\omega_m/2\pi = 1$ GHz, $\kappa_2/2\pi = 15$ MHz, $J = \frac{1}{2}\sqrt{\omega_m^2 + (\kappa_1+\kappa_2)^2/4}$, $\gamma_m/2\pi = 0.1$ MHz, $S = 1 \times 10^{10}$ [20,21,38].

Eq. (A5) in the Appendix]:

$$\dot{\tilde{m}} = -\gamma_m/2\tilde{m} + iG\sqrt{S/2}\,/2\tilde{\Phi}e^{i(\omega_m-\Delta\omega)t}, \tag{5a}$$

$$\dot{\tilde{\Phi}} = -\gamma'/2\tilde{\Phi} - iG\sqrt{S/2}\,\Delta N/2\tilde{m}e^{i(\Delta\omega-\omega_m)t}. \tag{5b}$$

Due to the fact that the optical decay is more rapid than the decay of magnons, i.e., κ_2, $\gamma' \gg \gamma_m$, comparing with the variation of $\tilde{\Phi}$, $\tilde{m}$ can be seen as constant. Namely, the degree of freedom of the optical mode can be adiabatically eliminated [31]. In addition, we consider the mean response of the intracavity photons and population difference ΔN due to the fact that the optical frequency is much larger than the magnon frequency. The time-dependent term of $\tilde{\Phi}$ resulting from the temporal evolution of ΔN can be safely neglected due to $\gamma' \gg G\sqrt{S}$ [31,52]. In order to satisfy the condition $\gamma' \gg \gamma_m$ and $G\sqrt{S}$, the maximum value that κ_1/κ_2 can achieve is 0.95 approximately. So we can solve Eq. (5b) analytically by the solution of a first-order ordinary differential equation and obtain the first-order approximate solution as follows:

$$\tilde{\Phi} = \frac{-iG\sqrt{S/2}\,\Delta N/2e^{i(\Delta\omega-\omega_m)t}}{i(\Delta\omega-\omega_m)+\frac{\gamma'}{2}}\tilde{m}. \tag{6}$$

By substituting $\tilde{\Phi}$ into Eq. (5a), the amplitude of magnon $\tilde{m}$ can be obtained as

$$\tilde{m} = \exp\left[(-\gamma_m/2 + \mathcal{G} - i\Omega_m)t\right], \tag{7}$$

with

$$\mathcal{G} = \text{Re}\left[\frac{G^2S\Delta N/8}{i(\Delta\omega-\omega_m)+\frac{\gamma'}{2}}\right] = \frac{G^2S\Delta N\gamma'/16}{(\Delta\omega-\omega_m)^2+\left(\frac{\gamma'}{2}\right)^2},$$

$$\Omega_m = \text{Im}\left[\frac{G^2S\Delta N/8}{i(\Delta\omega-\omega_m)+\frac{\gamma'}{2}}\right] = \frac{iG^2S\Delta N(\Delta\omega-\omega_m)/8}{(\Delta\omega-\omega_m)^2+\left(\frac{\gamma'}{2}\right)^2}. \tag{8}$$

$\mathcal{G}$ represents the magnon gain arising from the energy transition from a higher energy level ω_+ to a lower energy level ω_- accompanied by coherent amplification of stimulated emission of magnons. According to Eq. (7), the stimulated emission of magnon number $M(t) = |\tilde{m}|^2 = \exp[2(\mathcal{G} - \gamma_m/2)t]$. Setting $\tau = [\gamma_m/2]^{-1}$, we define $M(\tau) = \exp[2(\mathcal{G} - \gamma_m/2)/(\gamma_m/2)]$ as the magnon number at $t = [\gamma_m/2]^{-1}$, which characterizes the performance of the magnon laser.

III. RESULTS AND DISCUSSION

It is well known that an optical laser performs by the interaction between the pump field and the gain medium. Here, the two optical supermodes, acting as the gain medium, can produce stimulated emission of magnons driven by the pump field. Figure 3(a) shows that the magnon gain $\mathcal{G}$ changes with the incident power P_{in} and optical gain-loss ratio κ_1/κ_2. By setting the threshold condition $\mathcal{G} = \gamma_m/2$, we can obtain the threshold power P_{th} of the $\mathcal{PT}$-symmetric magnon laser, varying with κ_1/κ_2, which reveals the critical value of the driving power at which the magnon gain can overcome the dissipation of magnons. We can see that, with increasing optical gain coefficient κ_1, the magnitude of magnon gain increases dramatically. In contrast, the threshold power decreases extremely as κ_1 increases and is reduced to 21.6 mW when κ_1 reaches about $0.95\kappa_2$. According to previous studies, the balanced gain and loss condition ($\kappa_1/\kappa_2 \to 1$) can be careful satisfied by optically pumping the doped erbium ions in the active cavity to acquire the desired gain κ_1 [45]. The effective magnon gain is a necessary prerequisite of producing magnon laser action. Figure 3(b) shows that the magnon gain $\mathcal{G}$ varies with the incident power P_{in} and the optomagnonic coupling strength G. According to the relationship between the threshold power P_{th} and the optomagnonic coupling strength G depicted by the black solid line in Fig. 3(b), we can see that the threshold power becomes lower as the coupling strength increases; moreover, it features an exponential decay law approximately, which limits further reduction of the threshold power.

Figure 4 presents the stimulated emitted magnon number $M(\tau)$ versus the input power P_{in} for four different values of the cavity gain coefficient κ_1. The black solid line [$M(\tau) = 1$]

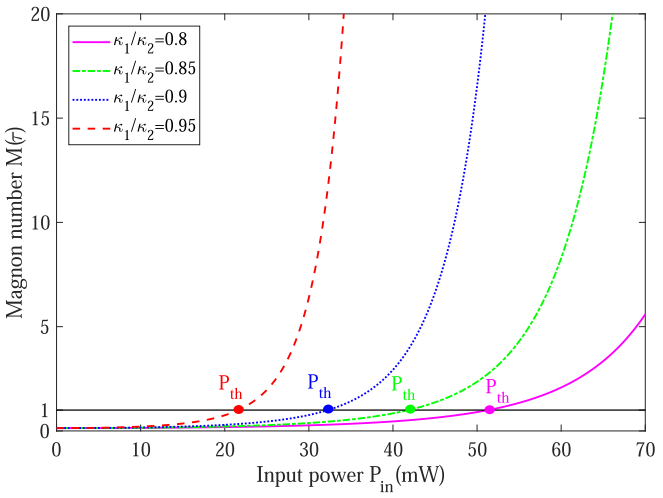

FIG. 4. Magnon laser as seen through the stimulated emitted magnon number $M(\tau)$ varied with the input power P_{in} for the different gain coefficients κ_1 under the matching condition $\Delta\omega = \omega_m$. The other system parameters are the same as Fig. 3(a).

represents the threshold condition obtained by $\mathcal{G} = \gamma_m/2$ and the four colored dots denote the threshold power respectively. The matching condition requires that the splitting of the two supermodes is resonant with the magnon frequency $\Delta\omega = \omega_m$, i.e., $2\sqrt{J^2 - (\kappa_1 + \kappa_2)^2/16} = \omega_m$, and the system accompanied by the strong optical tunneling rate between the active and passive cavities is well within the $\mathcal{PT}$-symmetric regime. Fundamentally, the magnon laser action is generated by a parametric resonance process, where the energy transition between the two optical supermodes $\omega_\pm$ can be engineered by magnons. Namely, a photon with higher energy is annihilated to generate a photon with lower energy and a magnon. This is consistent with the physical mechanism of optical laser generation, that is, the pump light interacts with the gain medium to excite the two-level system to emit coherent photons from the high level to the low level. Based on previous researches [31,43], only above the threshold value can the magnon laser occur. We can clearly see that the magnon number increases fast with the input power after reaching the threshold value, which indicates that the magnon laser is well triggered. Moreover, Fig. 4 also shows that one can tune κ_1 to adjust the threshold value of the magnon laser, and the magnon laser allows a low threshold value when the optical gain-loss ratio κ_1/κ_2 increasingly approaches 1. It clearly shows that $\kappa_1/\kappa_2 = 0.8, 0.85, 0.9, 0.95$, respectively, correspond to the threshold values $P_{\text{th}} = 51.3, 41.8, 32.3, 21.6$ mW. Physically, this is because, in the $\mathcal{PT}$-symmetry phase, the linewidth of the two optical supermodes ($\gamma_\pm$) is very small when the system approaches the optical gain-loss balance, resulting in the fact that the process of exchanging energy between the optical supermodes operates with low internal loss.

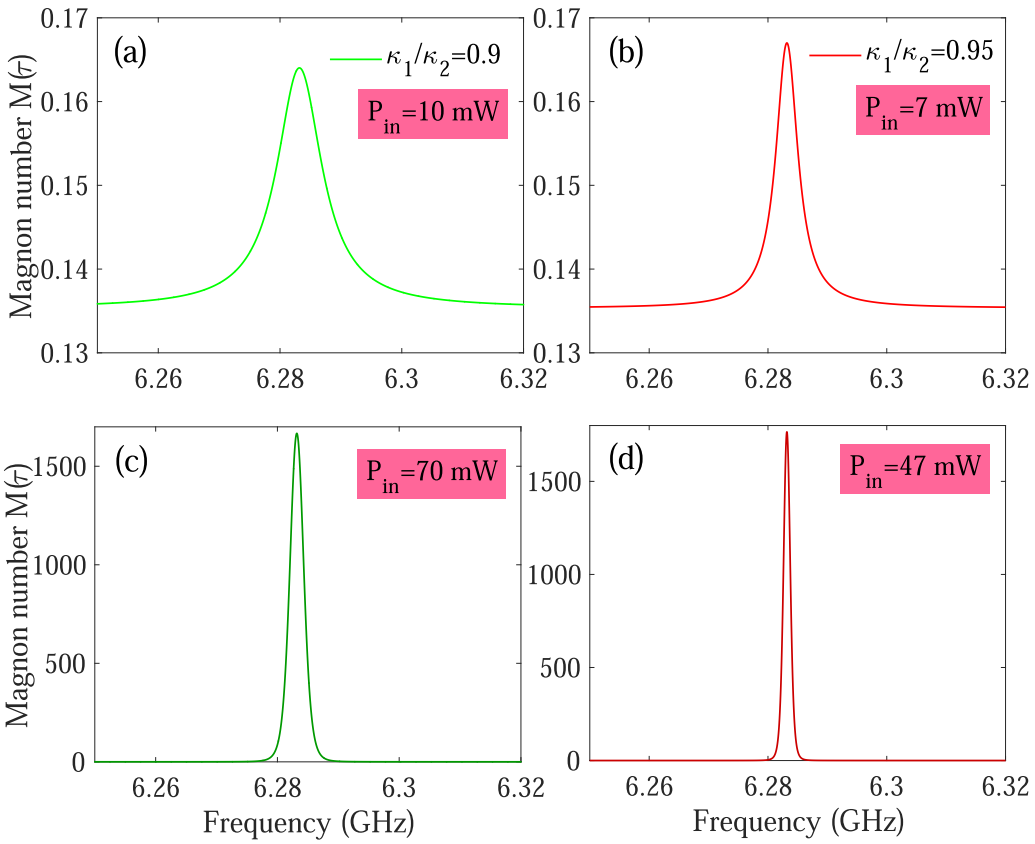

FIG. 5. The magnon emission line shape function below and above the threshold value in the context of gain-loss ratio $\kappa_1/\kappa_2 = 0.9$ [(a) and (c)] and $\kappa_1/\kappa_2 = 0.95$ [(b) and (d)]. The input powers in (a)–(d) are 10, 7, 70, and 47 mW respectively. The other system parameters are the same as Fig. 3(a).

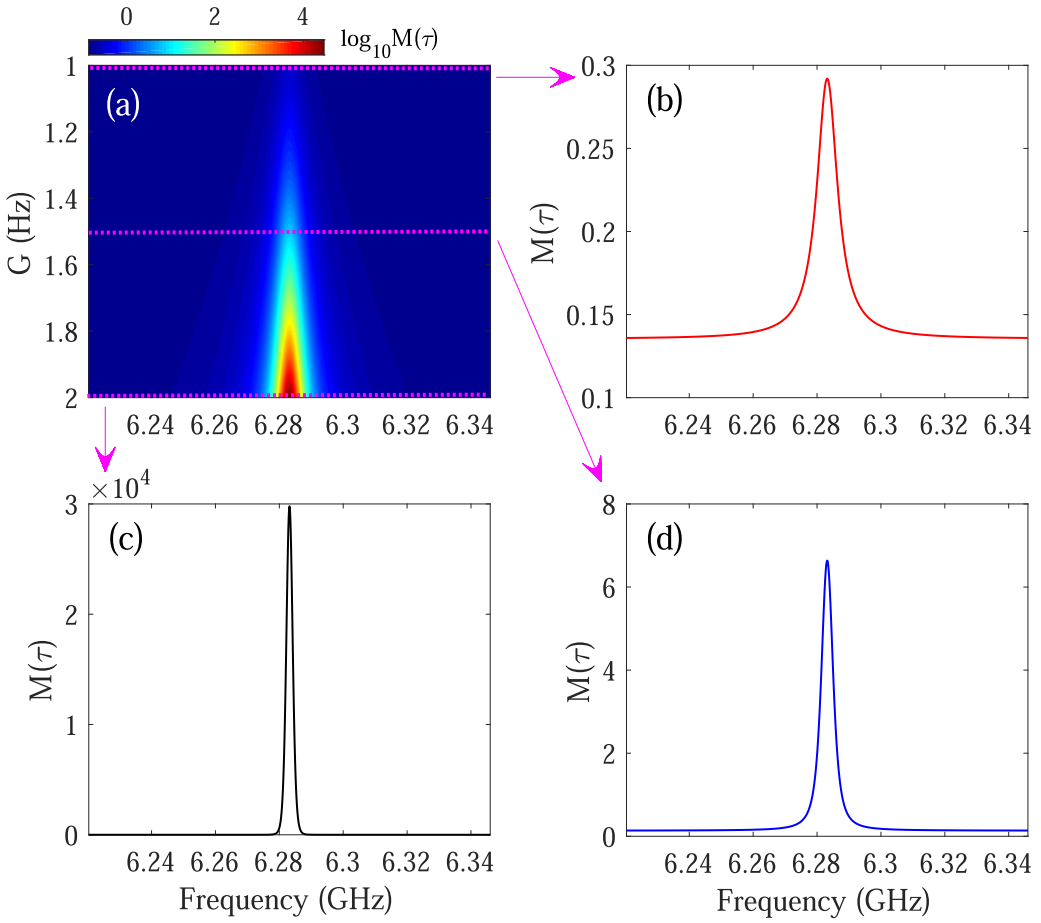

FIG. 6. (a) Stimulated emitted magnon number $M(\tau)$ (in logarithmic form) as a function of the optomagnonic coupling strength G and the laser frequency. (b)–(d) plot the magnon line shape function in the cases of $G = 1$, 2, and 1.5 Hz, respectively. We choose $P_{\text{in}} = 20$ mW, $\kappa_1/\kappa_2 = 0.9$, and the other system parameters are the same as Fig. 3.

Figure 5 shows the magnon emission line shape as a Gaussian function with center frequency $\omega_m = 6.283$ GHz below and above the threshold value. Based on the above analysis, the threshold values of $\kappa_1/\kappa_2 = 0.9,\ 0.95$ correspond to $P_{\text{th}} = 32.3$ and 21.6 mW respectively. By comparing Figs. 5(a) and 5(c), we can see that the linewidth above the threshold value is much narrower than that below the threshold value. And a similar phenomenon can be observed in Figs. 5(b) and 5(d). On the other hand, although Figs. 5(c) and 5(d) exhibit similar magnon numbers, the linewidth in Fig. 5(d) is significantly narrower. Specifically, the linewidth of the magnon laser with $\kappa_1/\kappa_2 = 0.9$ is about 3 MHz, while the linewidth is about 1 MHz with $\kappa_1/\kappa_2 = 0.95$. For the practical application, the narrower linewidth gives the magnon laser a better coherency property, which provides a promising route for achieving a high-intensity and narrow-pulse laser [56]. In addition, the average number of thermal magnons is about 6256 at $T = 300$ K by numerical calculation, while the stimulated emitted magnon number can achieve 1.32×10^6 approximately with $\kappa_1/\kappa_2 = 0.92$ when the input power is 80 mW. So we can ignore the influence of thermal noise safely at room temperature. This merit may bring about a new and broad prospective for the practical application of magnon lasers.

In order to more intuitively describe the relationship between stimulated emitted magnon number $M(\tau)$ and the optomagnonic coupling strength G, we plot a three-dimensional diagram of $M(\tau)$ (in logarithmic form) varying with the optomagnonic coupling strength G and the laser frequency in Fig. 6(a). As expected, the stronger optomagnonic coupling can improve the magnon laser generation. This is because the magnon gain is proportional to the square of the optomagnonic coupling strength G based on Eq. (8). In detail, Figs. 6(b)–6(d) show the magnon line shape function under the conditions of $G = 1$, 2, and 1.5 Hz, respectively. It can be seen that the enhancement of the optomagnonic coupling will lead not only to the dramatic enhancement of the magnon number, but to the reduction of the linewidth of the magnon laser. In the laboratory, one can scale down the YIG sphere size to reduce the mode volume to improve the coupling strength [18]. Furthermore, the spatial overlap between the magnons and photons can be engineered in ellipsoidal or nanostructured magnets to improve the coupling strength [19]. With these improvements and the above discussion, a magnon laser featuring narrow linewidth and low threshold can be highly accessible in experiments in the near future.

To further show the performance and tunability of the magnon laser, in Fig. 7, we present the dependence of the frequency distribution of the magnon laser on the applied magnetic field H_0 for the same driving power and gain-loss ratio. As can be seen from the figure, the magnetic fields

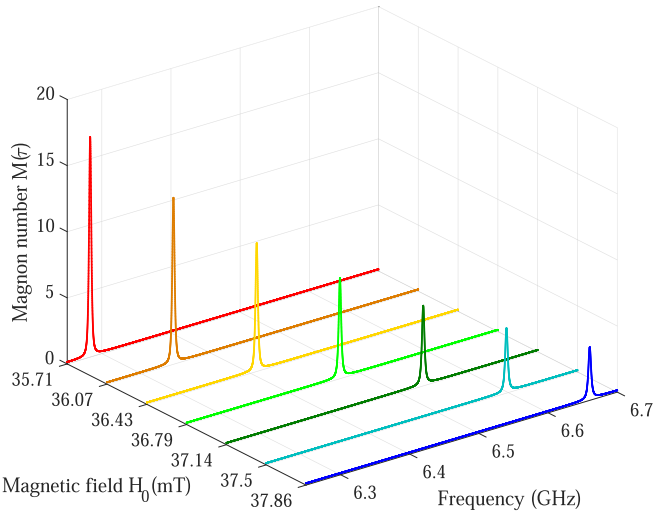

FIG. 7. The line shape function of stimulated emitted magnon number $M(\tau)$ in the case of different magnetic field strengths H_0. The curves with different colors, denoting the magnon lasers with different frequencies, correspond to the different applied magnetic fields. Here $\kappa_1/\kappa_2 = 0.9$, $P_{\text{in}} = 50$ mW, and the other system parameters are are the same as Fig. 3(a).

$H_0 = (35.71, 36.07, 36.43, 36.79, 37.14, 37.5, 37.86)$ mT, respectively, correspond to magnon laser frequencies $\omega_m = (6.283, 6.346, 6.409, 6.472, 6.535, 6.597, 6.66)$ GHz depicted by the different color curves. Although the magnon laser what we show in Fig. 7 is modulated in the form of equally spaced magnon modes, arbitrary frequencies of the magnon laser can be acquired by adjusting the magnetic field $H_0 = 2\sqrt{J^2 - (\kappa+\gamma)^2/16}/\gamma$ derived from $\Delta\omega = \omega_m = \gamma H_0$, which restricts the frequency splitting of the two supermodes based on the matching condition mentioned above. In general, the center frequency of the magnon emission line shape representing the frequency of the magnon laser can be well tuned by the applied magnetic field. The underlying physical mechanism is derived from the prominent controllability of the $\mathcal{PT}$-symmetric optical structure and optomagnonic system. Specifically, on the one hand, the frequency splitting of the two supermodes can be regulated by the coupling strength between the active cavity and passive cavity in the $\mathcal{PT}$-symmetric structure, which can be implemented by adjusting the distance between the active cavity and passive cavity in experiments [45]. And the splitting frequency can be tuned from 10 MHz to nearly 10 GHz by using microtoroids to enhance the evanescent coupling strength [52]. Furthermore, a recent experimental work suggests that a coupled magneto-optical microcavities structure can be used to improve the microwave-to-optical conversion efficiency, operating with the frequency splitting of the optical supermodes matching the magnon frequency [23]. On the other hand, the frequency of the magnon mode can be well mediated by the applied magnetic field. Thus, within current experimental reach, the frequency splitting can have a resonance with the magnon frequency in a wide frequency range (ranging from 1 to 10 GHz [42]) via tuning the magnon frequency and the coupling strength [23]. The flexible controllability of frequency gives the $\mathcal{PT}$-symmetric magnon laser more expansive application scenarios. According to previous studies, the frequency regulation of a laser is realized by the frequency-doubling process, such as high-order harmonic generation via the interaction between light and atom [57], high-order sideband generation via the mechanical effect of light [58], and so on. To the best of our knowledge, it is presently quite difficult for a laser device to realize continuous adjustment of laser frequency in a large operational bandwidth. Excitingly, this study makes a $\mathcal{PT}$-symmetric optomagnonic system an alternative candidate for engineering new laser devices with flexible frequency regulation, which may vigorously facilitate the magnon laser in fundamental scientific investigations and practical applications.

IV. CONCLUSION

In conclusion, we have theoretically proposed the concept of a $\mathcal{PT}$-symmetric magnon laser and explored its characteristics with respect to threshold and controllability. We show that the stimulated emitted magnon number can be coherently amplified in the $\mathcal{PT}$-symmetric regime and follows an exponential increase law, which indicates a magnon laser action. Moreover, by varying the applied magnetic field strength, the frequency of the magnon laser can be continuously adjusted in a frequency range distributed from about 1 to 10 GHz subject to the frequency of the Kittel magnon mode allowed in the ferrimagnet YIG sphere within current experimental reach. In addition, the approximately balanced optical gain-loss ratio makes the magnon laser perform at a low threshold. Based on the flexible controllability of our scheme, the magnon laser presented here possesses the features of low threshold and tunable frequency, which are urgently required for practical applications in engineering new chip-based laser devices. This study provides an achievable route for realizing continuous frequency regulation in a laser field by virtue of magnonics, and may promote the intersection and merging of $\mathcal{PT}$-symmetric theory and magnon spintronics.

ACKNOWLEDGMENTS

This work was supported by the National Natural Science Foundation of China (NSFC) (Grants No. 12004202 and No. 11975103), the Nanyang Basic and Frontier Research Project (Grant No. JCQY001), and Doctoral Research Start-up Funds of Nanyang Institute of Technology (NGBJ-2019-11).

APPENDIX: DERIVATION OF THE DYNAMICAL EQUATIONS

By introducing the supermode operators $\hat{a}_\pm = (\hat{a}_1 \pm \hat{a}_2)/\sqrt{2}$, the optomagnonic interaction of Hamiltonian $\hbar G\sqrt{S/2}\hat{a}_2^\dagger\hat{a}_2(\hat{m} + \hat{m}^\dagger)$ can be written as

$$\frac{\hbar G\sqrt{S/2}}{2}(\hat{a}_+^\dagger\hat{a}_+\hat{m}^\dagger - \hat{a}_-^\dagger a_+\hat{m}^\dagger - \hat{a}_+^\dagger\hat{a}_-\hat{m}^\dagger + \hat{a}_-^\dagger\hat{a}_-\hat{m}^\dagger + \hat{a}_+^\dagger\hat{a}_+\hat{m} - \hat{a}_-^\dagger a_+\hat{m} - \hat{a}_+^\dagger\hat{a}_-\hat{m} + \hat{a}_-^\dagger\hat{a}_-\hat{m}). \quad \text{(A1)}$$

Applying the rotating-wave approximation, the Hamiltonian (A1) becomes

$$-\frac{\hbar G\sqrt{S/2}}{2}(\hat{a}_-^\dagger a_+\hat{m}^\dagger + \hat{a}_+^\dagger \hat{a}_-\hat{m}). \tag{A2}$$

So the Hamiltonian Eq. (1) can be converted to

$$\hat{H} = \hbar\omega_+\hat{a}_+^\dagger\hat{a}_+ + \hbar\omega_-\hat{a}_-^\dagger\hat{a}_- + \hbar\omega_m\hat{m}^\dagger\hat{m} - \frac{\hbar G\sqrt{S/2}}{2}(\hat{a}_-^\dagger\hat{a}_+\hat{m}^\dagger + \hat{a}_+^\dagger\hat{a}_-\hat{m}) + i\hbar\sqrt{\kappa}/2\Omega_d(\hat{a}_+^\dagger + \hat{a}_-^\dagger - \text{H.c.}). \tag{A3}$$

Based on the above Hamiltonian, the semiclassical Heisenberg-Langevin equations read (setting $A = \langle\hat{A}\rangle$, where A is an any magnon or optical inversion operator)

$$\dot{m} = (-i\omega_m - \gamma_m/2)m + iG\sqrt{S/2}\,/2\Phi, \tag{A4a}$$

$$\dot{\Phi} = (-i\Delta\omega - \gamma'/2)\Phi - iG\sqrt{S/2}\,\Delta N/2m. \tag{A4b}$$

Transferring the variables m and Φ to a rotating frame by carrying out an unitary transformation $U(t) = \exp(i\omega_m m^\dagger m t + i\Delta\omega\Phi^\dagger\Phi t)$, we can obtain

$$\tilde{m} = U^\dagger m U = me^{i\omega_m t}, \quad \tilde{\Phi} = U^\dagger\Phi U = \Phi e^{i\Delta\omega t}. \tag{A5}$$

By substituting Eq. (A5) into Eqs. (A4), we can obtain

$$\dot{\tilde{m}} = -\gamma_m/2\tilde{m} + iG\sqrt{S/2}\,/2\tilde{\Phi}e^{i(\omega_m-\Delta\omega)t}, \tag{A6a}$$

$$\dot{\tilde{\Phi}} = -\gamma'/2\tilde{\Phi} - iG\sqrt{S/2}\,\Delta N/2\tilde{m}e^{i(\Delta\omega-\omega_m)t}. \tag{A6b}$$

[1] A. V. Chumak, V. I. Vasyuchka, A. A. Serga, and B. Hillebrands, Magnon spintronics, Nat. Phys. **11**, 453 (2015).

[2] O. O. Soykal and M. E. Flatte, Strong Field Interactions between a Nanomagnet and a Photonic Cavity, Phys. Rev. Lett. **104**, 077202 (2010).

[3] X.-F. Zhang, C.-L. Zou, L. Jiang, and H. X. Tang, Strongly Coupled Magnons and Cavity Microwave Photons, Phys. Rev. Lett. **113**, 156401 (2014).

[4] L. H. Bai, M. Harder, Y. P. Chen, X. Fan, J. Q. Xiao, and C.-M. Hu, Spin Pumping in Electrodynamically Coupled Magnon-Photon Systems, Phys. Rev. Lett. **114**, 227201 (2015).

[5] Y. Tabuchi, S. Ishino, T. Ishikawa, R. Yamazaki, K. Usami, and Y. Nakamura, Hybridizing Ferromagnetic Magnons and Microwave Photons in the Quantum Limit, Phys. Rev. Lett. **113**, 083603 (2014).

[6] Y.-P. Wang, G.-Q. Zhang, D. Zhang, T.-F. Li, C.-M. Hu, and J.-Q. You, Bistability of Cavity Magnon Polaritons, Phys. Rev. Lett. **120**, 057202 (2018).

[7] D. Zhang, X.-M. Wang, T.-F. Li, X.-Q. Luo, W. Wu, F. Nori, and J. Q. You, Cavity quantum electrodynamics with ferromagnetic magnons in a small yttrium-iron-garnet sphere, npj Quantum Inf. **1**, 15014 (2015).

[8] Z.-B. Yang, H. Jin, J.-W. Jin, J.-Y. Liu, H.-Y. Liu, and R.-C. Yang, Bistability of squeezing and entanglement in cavity magnonics, Phys. Rev. Research **3**, 023126 (2021).

[9] J. Zhao, Y. Liu, L. Wu, C.-K. Duan, Y.-x. Liu, and J. Du, Observation of Anti-$\mathcal{PT}$-Symmetry Phase Transition in the Magnon-Cavity-Magnon Coupled System, Phys. Rev. Appl. **13**, 014053 (2020).

[10] Y.-P. Wang, J. W. Rao, Y. Yang, P.-C. Xu, Y. S. Gui, B. M. Yao, J. Q. You, and C.-M. Hu, Nonreciprocity and Unidirectional Invisibility in Cavity Magnonics, Phys. Rev. Lett. **123**, 127202 (2019).

[11] X. Zhang, C.-L. Zou, L. Jiang, and H. X. Tang, Cavity magnomechanics, Sci. Adv. **2**, e1501286 (2016).

[12] J. Li, S.-Y. Zhu, and G. S. Agarwal, Magnon-Photon-Phonon Entanglement in Cavity Magnomechanics, Phys. Rev. Lett. **121**, 203601 (2018).

[13] C. Kong, B. Wang, Z.-X. Liu, H. Xiong, and Y. Wu, Magnetically controllable slow light based on magnetostrictive forces, Opt. Express **27**, 5544 (2019).

[14] T.-X. Lu, H. Zhang, Q. Zhang, and H. Jing, Exceptional-point-engineered cavity magnomechanics, Phys. Rev. A **103**, 063708 (2021).

[15] Y. Tabuchi, S. Ishino, A. Noguchi, T. Ishikawa, R. Yamazaki, K. Usami, and Y. Nakamura, Coherent coupling between a ferromagnetic magnon and a superconducting qubit, Science **349**, 405 (2015).

[16] D. Lachance-Quirion, Y. Tabuchi, S. Ishino, A. Noguchi, T. Ishikawa, R. Yamazaki, and Y. Nakamura, Resolving quanta of collective spin excitations in a millimeter-sized ferromagnet, Sci. Adv. **3**, e1603150 (2017).

[17] Z.-X. Liu, H. Xiong, and Y. Wu, Magnon blockade in a hybrid ferromagnet-superconductor quantum system, Phys. Rev. B **100**, 134421 (2019).

[18] A. Osada, R. Hisatomi, A. Noguchi, Y. Tabuchi, R. Yamazaki, K. Usami, M. Sadgrove, R. Yalla, M. Nomura, and Y. Nakamura, Cavity Optomagnonics with Spin-Orbit Coupled Photons, Phys. Rev. Lett. **116**, 223601 (2016).

[19] S. Sharma, B. Z. Rameshti, Y. M. Blanter, and G. E. W. Bauer, Optimal mode matching in cavity optomagnonics, Phys. Rev. B **99**, 214423 (2019).

[20] S. V. Kusminskiy, H. X. Tang, and F. Marquardt, Coupled spin-light dynamics in cavity optomagnonics, Phys. Rev. A **94**, 033821 (2016).

[21] X. Zhang, N. Zhu, C.-L. Zou, and H. X. Tang, Optomagnonic Whispering Gallery Microresonators, Phys. Rev. Lett. **117**, 123605 (2016).

[22] R. Hisatomi, A. Osada, Y. Tabuchi, T. Ishikawa, A. Noguchi, R. Yamazaki, K. Usami, and Y. Nakamura, Bidirectional conversion between microwave and light via ferromagnetic magnons, Phys. Rev. B **93**, 174427 (2016).

[23] C.-Z. Chai, Z. Shen, Y.-L. Zhang, H.-Q. Zhao, G.-C. Guo, C.-L. Zou, and C.-H. Dong, Single-sideband microwave-to-optical conversion in high-Q ferrimagnetic microspheres, Photonics Res. **10**, 820-827 (2022).

[24] A. Osada, A. Gloppe, R. Hisatomi, A. Noguchi, R. Yamazaki, M. Nomura, Y. Nakamura, and K. Usami, Brillouin Light Scattering by Magnetic Quasivortices in Cavity Optomagnonics, Phys. Rev. Lett. **120**, 133602 (2018).

[25] W.-J. Wu, Y.-P. Wang, J.-Z. Wu, J. Li, and J. Q. You, Remote magnon entanglement between two massive ferrimagnetic spheres via cavity optomagnonics, Phys. Rev. A **104**, 023711 (2021).

[26] T. Liu, X. Zhang, H. X. Tang, and M. E. Flatté, Optomagnonics in magnetic solids, Phys. Rev. B **94**, 060405(R) (2016).

[27] B. Wang, Z.-X. Liu, C. Kong, H. Xiong, and Y. Wu, Magnon-induced transparency and amplification in $\mathcal{PT}$-symmetric cavity-magnon system, Opt. Express **26**, 20248 (2018).

[28] W.-L. Xu, Y.-P. Gao, C. Cao, T.-J. Wang, and C. Wang, Nanoscatterer-mediated frequency combs in cavity optomagnonics, Phys. Rev. A **102**, 043519 (2020).

[29] W.-L. Xu, X.-F. Liu, Y. Sun, Y.-P. Gao, T.-J. Wang, and C. Wang, Magnon-induced chaos in an optical $\mathcal{PT}$-symmetric resonator, Phys. Rev. E **101**, 012205 (2020).

[30] Z.-X. Liu, C. You, B. Wang, H. Xiong, and Y. Wu, Phase-mediated magnon chaos-order transition in cavity optomagnonics, Opt. Lett. **44**, 507 (2019).

[31] H. Jing, S. K. Özdemir, X.-Y. Lü, J. Zhang, L. Yang, and F. Nori, $\mathcal{PT}$-Symmetric Phonon Laser, Phys. Rev. Lett. **113**, 053604 (2014).

[32] X.-Y. Lü, H. Jing, J. Ma, and Y. Wu, $\mathcal{PT}$-Symmetry-Breaking Chaos in Optomechanics, Phys. Rev. Lett. **114**, 253601 (2015).

[33] H. Zhang, R. Huang, S.-D. Zhang, Y. Li, C.-W. Qiu, F. Nori, and H. Jing, Breaking anti-$\mathcal{PT}$ symmetry by spinning a resonator, Nano Lett. **20**, 7594 (2020).

[34] D. Zhang, X.-Q. Luo, Y.-P. Wang, T.-F. Li, and J. Q. You, Observation of the exceptional point in cavity magnon polaritons, Nat. Commun. **8**, 1368 (2017).

[35] G.-Q. Zhang, Z. Chen, D. Xu, N. Shammah, M. Liao, T.-F. Li, L. Tong, S.-Y. Zhu, F. Nori, and J. Q. You, Exceptional point and cross-relaxation effect in a hybrid quantum system, PRX Quantum **2**, 020307 (2021).

[36] Y. Yang, Yi-Pu Wang, J. W. Rao, Y. S. Gui, B. M. Yao, W. Lu, and C.-M. Hu, Cavity Optomagnonics with Spin-Orbit Coupled Photons, Phys. Rev. Lett. **125**, 147202 (2020).

[37] Y. Cao, and P. Yan, Exceptional magnetic sensitivity of $\mathcal{PT}$-symmetric cavity magnon polaritons, Phys. Rev. B **99**, 214415 (2019).

[38] Z.-X. Liu, and H. Xiong, Magnon laser based on Brillouin light scattering, Opt. Lett. **45**, 5452 (2020).

[39] Y.-J. Xu and J. Song, Nonreciprocal magnon laser, Opt. Lett. **46**, 5276 (2021).

[40] J. B. Khurgin, M. Clerici, V. Bruno, L. Caspani, C. DeVault, J. Kim, A. Shaltout, A. Boltasseva, V. M. Shalaev, M. Ferrera, D. Faccio, and N. Kinsey, Adiabatic frequency shifting in epsilon-near-zero materials: the role of group velocity, Optica **7**, 226 (2020).

[41] S. Mahashabde, E. Otto, D. Montemurro, S. Graaf, S. Kubatkin, and A. Danilov, Fast Tunable High-Q-Factor Superconducting Microwave Resonators, Phys. Rev. Appl. **14**, 044040 (2020).

[42] S. Sharma, Y. M. Blanter, and G. E. W. Bauer, Light scattering by magnons in whispering gallery mode cavities, Phys. Rev. B **96**, 094412 (2017).

[43] B. Wang, Z.-X. Liu, X. Jia, H. Xiong, and Y. Wu, Polarization-based control of phonon laser action in a Parity Time-symmetric optomechanical system, Commun. Phys. **1**, 43 (2018).

[44] M. Jäckl, V. I. Belotelov, I. A. Akimov, I. V. Savochkin, D. R. Yakovlev, A. K. Zvezdin, and M. Bayer, Magnon Accumulation by Clocked Laser Excitation as Source of Long-Range Spin Waves in Transparent Magnetic Films, Phys. Rev. X **7**, 021009 (2017).

[45] B. Peng, S. K. Özdemir, F. Lei, F. Monifi, M. Gianfreda, G. L. Long, S. Fan, F. Nori, C. M. Bender, and L. Yang, Parity-time-symmetric whispering-gallery microcavities, Nat. Phys. **10**, 394 (2014).

[46] L. Chang, X. Jiang, S. Hua, C. Yang, J. Wen, L. Jiang, G. Li, G. Wang, and M. Xiao, Parity-time symmetry and variable optical isolation in active-passive-coupled microresonators, Nat. Photonics **8**, 524 (2014).

[47] T. Holstein and H. Primakoff, Field dependence of the intrinsic domain magnetization of a ferromagnet, Phys. Rev. **58**, 1098 (1940).

[48] H. Xiong, J.-H. Gan, and Y. Wu, Kuznetsov-Ma Soliton Dynamics Based on the Mechanical Effect of Light, Phys. Rev. Lett. **119**, 153901 (2017).

[49] H. Xiong, Y.-M. Huang, and Y. Wu, Laguerre-Gaussian optical sum-sideband generation via orbital angular momentum exchange, Phys. Rev. A **103**, 043506 (2021).

[50] D. F. Walls and G. J. Milburn, *Quantum Optics* (Springer, Berlin, 2008).

[51] C. W. Gardiner and P. Zoller, *Quantum Noise* (Springer, Berlin 2000).

[52] I. S. Grudinin, H. Lee, O. Painter, and K. J. Vahala, Phonon Laser Action in a Tunable Two-Level System, Phys. Rev. Lett. **104**, 083901 (2010).

[53] J. Graf, S. Sharma, H. Huebl, and S. Viola Kusminskiy, Design of an optomagnonic crystal: Towards optimal magnon-photon mode matching at the microscale, Phys. Rev. Research **3**, 013277 (2021).

[54] J. A. Haigh, R. A. Chakalov, and A. J. Ramsay, Subpicoliter Magnetoptical Cavities, Phys. Rev. Appl. **14**, 044005 (2020).

[55] N. Zhu, X. Zhang, X. Han, C.-L. Zou, C. Zhong, C.-H. Wang, L. Jiang, and H. X. Tang, Waveguide cavity optomagnonics for microwave-to-optics conversion, Optica **7**, 1291 (2020).

[56] D. Akamatsu, Y. Nakajima, H. Inaba, K. Hosaka, M. Yasuda, A. Onae, and F.-L. Hong, Narrow linewidth laser system realized by linewidth transfer using a fiber-based frequency comb for the magneto-optical trapping of strontium, Opt. Express **20**, 16010 (2012).

[57] A. L'Huillier and P. Balcou, High-Order Harmonic Generation in Rare Gases with a 1-ps 1053-nm Laser, Phys. Rev. Lett. **70**, 774 (1993).

[58] H. Xiong, L.-G. Si, X.-Y. Lü, X. Yang, and Y. Wu, Carrier-envelope phase-dependent effect of high-order sideband generation in ultrafast driven optomechanical system, Opt. Lett. **38**, 353 (2013).